Chapter 2

Single-particle states in typical quantum-dot confinements

Before I can move on to describing the many-particle properties of QDs, I first need to understand their single-particle spectra. In Chapter 1 I have shown that QDs can be fabricated in a variety of sizes and shapes, and the lateral confinement produced by each of them possesses its own characteristic symmetry properties. Detailed calculations, fully accounting for all the details of particular structures, are complicated and require large computational effort [26, 28, 70, 99, 112]. In this work, however, I shall approximate the complicated QD confinements by model potentials, capturing the fundamental physics, but at the same time making it possible to understand it in simple terms. I shall consider three fundamental classes of "ideal" QD geometries: (i) parabolic QDs, (ii) disk-shaped QDs, and (iii) quantum rings. It turns out, in fact, that these potentials are reasonably good approximations of the real QD potentials, so much so that in most cases it is sufficient to treat the peculiarities of each QD as small perturbations to the ideal shape [34, 70]. The two-dimensional parabolic potential is commonly used in modelling of gated quantum dot devices, both vertical [92, 121, 122] and lateral [31, 32, 33]. It has

also been successfully applied to lens-shaped self-assembled QDs (obtained without using the indium-flush technique) [34, 50, 57]. In this work, however, when talking about SADs I shall refer to the indium-flushed structures, whose geometry is approximated better by the disk-shaped potential. Finally, when discussing the quantum ring geometry I shall assume that this ring is of infinitesimal thickness, i.e., it is a one-dimensional circular system. This Chapter is devoted to describing and comparing the single-particle energy spectra of these three fundamental lateral confinements.

2.1 Parabolic lateral confinement

First I consider two-dimensional parabolic confinement in the presence of an external magnetic field $\mathbf{B} = [0, 0, B]$ perpendicular to the plane in which the potential is defined (by default, the XY plane). The Hamiltonian of a single electron in this case attains the following form:

$$\hat{H} = \frac{1}{2m^*}\left(\hat{\mathbf{p}} + \frac{e}{c}\hat{\mathbf{A}}\right)^2 + \frac{1}{2}m^*\omega_0^2 r^2 - g\mu_B B\sigma, \tag{2.1}$$

where m^* and e is the electron's effective mass and charge, respectively ($e > 0$; the negative sign of the charge is accounted for by the "+" sign in the first term), c is the velocity of light, and ω_0 is the characteristic frequency of the confining potential (CGS units are used). The last term of this Hamiltonian is the Zeeman term, with g being the Landé factor, $\mu_B = e\hbar/2m_e$ - the Bohr magneton, and $\sigma = \pm\frac{1}{2}$ - the z component of the electronic spin. Since the Zeeman term depends only on the spin component of the electronic wave function, I shall neglect it in the following calculations, and return to it in the discussion of results.

The problem at hand has been solved by Fock [44] and Darwin [37], and this is why the single-particle energy spectrum of such a parabolic potential is called the *Fock-Darwin spectrum.* The cited authors solved the Schrödinger equation with the Hamiltonian (2.1) in real space. I shall follow a different path, involving the harmonic-oscillator raising and

lowering operators. My description is similar to that given in Refs. [51, 62, 127].

To proceed I must first define the form of the vector potential $\mathbf{A}$. I choose the symmetric gauge: $\mathbf{A} = [-By/2, Bx/2, 0]$. To prove that this potential indeed corresponds to the vertical magnetic field $\mathbf{B}$ as specified above, I calculate

$$\nabla \times \mathbf{A} = \begin{vmatrix} \hat{i} & \hat{j} & \hat{k} \\ \frac{\partial}{\partial x} & \frac{\partial}{\partial y} & \frac{\partial}{\partial z} \\ -By/2 & Bx/2 & 0 \end{vmatrix} = \hat{k}(B+B)/2 = [0,0,B]. \tag{2.2}$$

Let us expand the expression $\left(\hat{\mathbf{p}} + \frac{e}{c}\hat{\mathbf{A}}\right)^2$ using the above vector potential:

$$\left(\hat{\mathbf{p}} + \frac{e}{c}\hat{\mathbf{A}}\right)^2 = \hat{\mathbf{p}}^2 + \frac{eB}{2c}(-p_x y + p_y x) + \frac{eB}{2c}(-y p_x + x p_y) + \frac{e^2B^2}{4c^2}(x^2+y^2).$$

Let us now define the cyclotron frequency $\omega_c = eB/m^*c$ (for GaAs, the cyclotron energy $\hbar\omega_c \approx 1.728$ meV for the magnetic field $B = 1$ T, and scales linearly with the field). Taking into account that $yp_x = p_x y$ and $xp_y = p_y x$, I get

$$\left(\hat{\mathbf{p}} + \frac{e}{c}\hat{\mathbf{A}}\right)^2 = \hat{\mathbf{p}}^2 + \frac{1}{4}(m^*)^2\omega_c^2\mathbf{r}^2 + m^*\omega_c\hat{l}_z,$$

where $\hat{l}_z = p_y x - p_x y$ is the z-th component of the angular momentum operator. The Hamiltonian can be now written in the following form:

$$\hat{H} = \frac{1}{2m^*}\hat{\mathbf{p}}^2 + \frac{1}{2}m^*\left(\omega_0^2 + \frac{1}{4}\omega_c^2\right)\mathbf{r}^2 + \frac{1}{2}\omega_c\hat{l}_z. \tag{2.3}$$

Using the notation $\left(\omega_0^2 + \frac{1}{4}\omega_c^2\right) = \omega_h^2$ ("hybrid frequency"), I get

$$\hat{H} = \frac{1}{2m^*}\hat{\mathbf{p}}^2 + \frac{1}{2}m^*\omega_h^2\mathbf{r}^2 + \frac{1}{2}\omega_c\hat{l}_z. \tag{2.4}$$

Let us further introduce complex variables:

$$z = x - iy, \qquad z^* = x + iy;$$
$$\partial_z = \partial_x + i\partial_y, \quad \partial_z^* = \partial_x - i\partial_y;$$

and write the position and gradient in their terms:

$$x = \tfrac{1}{2}(z+z^*), \qquad y = \tfrac{1}{2i}(z^*-z);$$
$$\partial_x = \tfrac{1}{2}(\partial_z + \partial_z^*), \quad \partial_y = \tfrac{1}{2i}(\partial_z - \partial_z^*).$$

It is straightforward to see that $x^2+y^2 = zz^*$ and $\partial_x^2+\partial_y^2 = \partial_z\partial_z^*$. Since $\hat{\mathbf{p}}^2 = -\hbar^2(\partial_x^2+\partial_y^2)$, the Hamiltonian in the new coordinates attains the form:

$$\hat{H} = -\frac{\hbar^2}{2m^*}(\partial_z\partial_z^*) + \frac{1}{2}m^*\omega_h^2(zz^*) - \frac{1}{4}\hbar\omega_c(z\partial_z - z^*\partial_z^*). \tag{2.5}$$

Next step is to define a unit length characteristic for this potential. I take $\ell = \sqrt{\frac{\hbar}{2m^*\omega_h}}$. Note that in zero magnetic field $\omega_h = \omega_0$ and $\ell_{B=0} = \sqrt{\frac{\hbar}{2m^*\omega_0}}$. In the absence of the parabolic confinement, but in the presence of the magnetic field, I get $\ell_B = \sqrt{\frac{\hbar}{m^*\omega_c}}$ (the magnetic length). Let us now insert this unit length into the Hamiltonian. The new, dimensionless variables are: $z_{new} = z_{old}/\ell$ and $\partial_{z(new)} = \partial_{z(old)}\ell$. Dropping the label "new" I get:

$$\hat{H} = -\frac{\hbar^2}{2m^*\ell^2}(\partial_z\partial_z^*) + \frac{1}{2}m^*\omega_h^2\ell^2(zz^*) - \frac{1}{4}\hbar\omega_c(z\partial_z - z^*\partial_z^*) \tag{2.6}$$

(in the last term no new factors appear, since ℓ crosses out). If I insert the explicit forms of ℓ, I obtain

$$\hat{H} = \hbar\omega_h(\frac{1}{4}zz^* - \partial_z\partial_z^*) - \frac{1}{4}\hbar\omega_c(z\partial_z - z^*\partial_z^*). \tag{2.7}$$

Let us now introduce the raising and lowering operators:

$$\begin{aligned} a &= \tfrac{1}{2}\left(\tfrac{z}{\sqrt{2}} + \partial_z^*\sqrt{2}\right), \quad a^+ = \tfrac{1}{2}\left(\tfrac{z^*}{\sqrt{2}} - \partial_z\sqrt{2}\right), \\ b &= \tfrac{1}{2}\left(\tfrac{z^*}{\sqrt{2}} + \partial_z\sqrt{2}\right), \quad b^+ = \tfrac{1}{2}\left(\tfrac{z}{\sqrt{2}} - \partial_z^*\sqrt{2}\right). \end{aligned} \tag{2.8}$$

To examine their properties I check two out of six of their possible commutators.

1. Commutator $[a, a^+]$.

$$[a, a^+] = \frac{1}{4}\left\{\left(\frac{1}{2}zz^* - z\partial_z + \partial_z^*z^* - 2\partial_z^*\partial_z\right) - \left(\frac{1}{2}z^*z - \partial_z z + z^*\partial_z^* - 2\partial_z\partial_z^*\right)\right\}.$$

But z commutes with z^* and ∂_z commutes with ∂_z^*, so the respective "pure" products cross out. Further, the commutator $[\partial_z, z] = 2$ and $[\partial_z^*, z^*] = 2$, so

$$[a, a^+] = 1.$$

Similarly one can prove that

$$[b, b^+] = 1.$$

2. Commutator $[a, b^+]$.

$$[a, b^+] = \frac{1}{4}\left\{\left(\frac{1}{2}z^2 - z\partial_z^* + \partial_z^* z - 2(\partial_z^*)^2\right) - \left(\frac{1}{2}z^2 - \partial_z^* z + z\partial_z^* - 2(\partial_z^*)^2\right)\right\}.$$

Again, the respective "pure" products cross out. Moreover, the commutator $[\partial_z^*, z] = 0$ and $[\partial_z, z^*] = 0$, so

$$[a, b^+] = 0.$$

Similarly one can prove that any commutator of a (a^+) with b (b^+) is zero.

Thus I have shown that the pairs of operators (a, a^+) and (b, b^+) are independent.

I shall express the Hamiltonian in terms of these operators. To this end I need to perform the inverse transformation:

$$\begin{aligned} z &= \sqrt{2}(a + b^+), \quad z^* = \sqrt{2}(a^+ + b), \\ \partial_z &= \tfrac{1}{\sqrt{2}}(b - a^+), \quad \partial_z^* = \tfrac{1}{\sqrt{2}}(a - b^+). \end{aligned} \tag{2.9}$$

Upon substitution into the Hamiltonian I obtain:

$$\begin{aligned} \hat{H} &= \frac{1}{2}\hbar\omega_h\left((a + b^+)(a^+ + b) - (b - a^+)(a - b^+)\right) \\ &- \frac{1}{4}\hbar\omega_c\left((a + b^+)(b - a^+) - (a^+ + b)(a - b^+)\right), \end{aligned} \tag{2.10}$$

and, after reduction,

$$\hat{H} = \hbar\omega_h\left(a^+a + \frac{1}{2}\right) + \hbar\omega_h\left(b^+b + \frac{1}{2}\right) + \frac{1}{2}\hbar\omega_c\left(a^+a + \frac{1}{2}\right) - \frac{1}{2}\hbar\omega_c\left(b^+b + \frac{1}{2}\right). \tag{2.11}$$

I can now define a pair of oscillator frequencies

$$\omega_\pm = \omega_h \pm \frac{1}{2}\omega_c, \tag{2.12}$$

and, in terms of these frequencies,

$$\hat{H} = \hbar\omega_+\left(a^+a + \frac{1}{2}\right) + \hbar\omega_-\left(b^+b + \frac{1}{2}\right). \tag{2.13}$$

Thus I have obtained a Hamiltonian of two harmonic oscillators. In analogy to the linear harmonic oscillator [35], the eigenstates of this Hamiltonian can be written as

$$|nm\rangle = \frac{1}{\sqrt{n!m!}}\left(a^+\right)^n\left(b^+\right)^m|00\rangle, \tag{2.14}$$

with n, m being quantum numbers ($n,\ m = 0, 1, 2, \ldots$). The lowering and raising operators acting on such state give

$$\begin{aligned} a|n,m\rangle &= \sqrt{n}|n-1,m\rangle, \quad a^+|n,m\rangle = \sqrt{n+1}|n+1,m\rangle; \\ b|n,m\rangle &= \sqrt{m}|n,m-1\rangle, \quad b^+|n,m\rangle = \sqrt{m+1}|n,m+1\rangle. \end{aligned} \tag{2.15}$$

I am now ready to write the formula for the energy of the eigenstate $|n,m\rangle$:

$$\varepsilon(n,m) = \hbar\omega_+\left(n+\frac{1}{2}\right) + \hbar\omega_-\left(m+\frac{1}{2}\right). \tag{2.16}$$

Let us now include the Zeeman term, introduced in the beginning of this Section, but neglected afterwards. This term accounts for the fact that the electron also has the spin degree of freedom, and its eigenstate should be identified by three quantum numbers: $|nm\sigma\rangle$, where $\sigma = \pm\frac{1}{2}$ is the quantum number describing the z spin component. In this case the electronic eigenenergies are

$$\varepsilon(n,m,\sigma) = \hbar\omega_+\left(n+\frac{1}{2}\right) + \hbar\omega_-\left(m+\frac{1}{2}\right) - g\mu_B B\sigma. \tag{2.17}$$

In Figure 2.1 I show a few lowest-lying energies $\varepsilon(n,m,\sigma)$ as a function of the magnetic field. In this calculation I take $\hbar\omega_0 = 6$ meV and the Landé factor $g = -4.4$. This value of $\hbar\omega_0$ is characteristic for the vertical dots in GaAs, but my Landé factor is one order of magnitude larger than that of GaAs ($g_{GaAs} = -0.44$). Thus the Zeeman energy $E_Z = |g\mu_B B|$ is artificially enhanced; I have done so in order to make the spin splitting visible on this energy scale.

At zero magnetic field I have $\omega_+ = \omega_- = \omega_0$ and

$$\varepsilon_{B=0}(n,m,\sigma) = \hbar\omega_0(n+m+1), \tag{2.18}$$

i.e., the energy of all eigenstates with the same value of $n+m$ is the same. These are the degenerate *shells;* let us name a few of them here. The lowest one, called the s shell, consists of two states, both with $n = m = 0$, but with different σ (i.e., the s shell is doubly degenerate with respect to spin). The second one, called the p shell, consists of

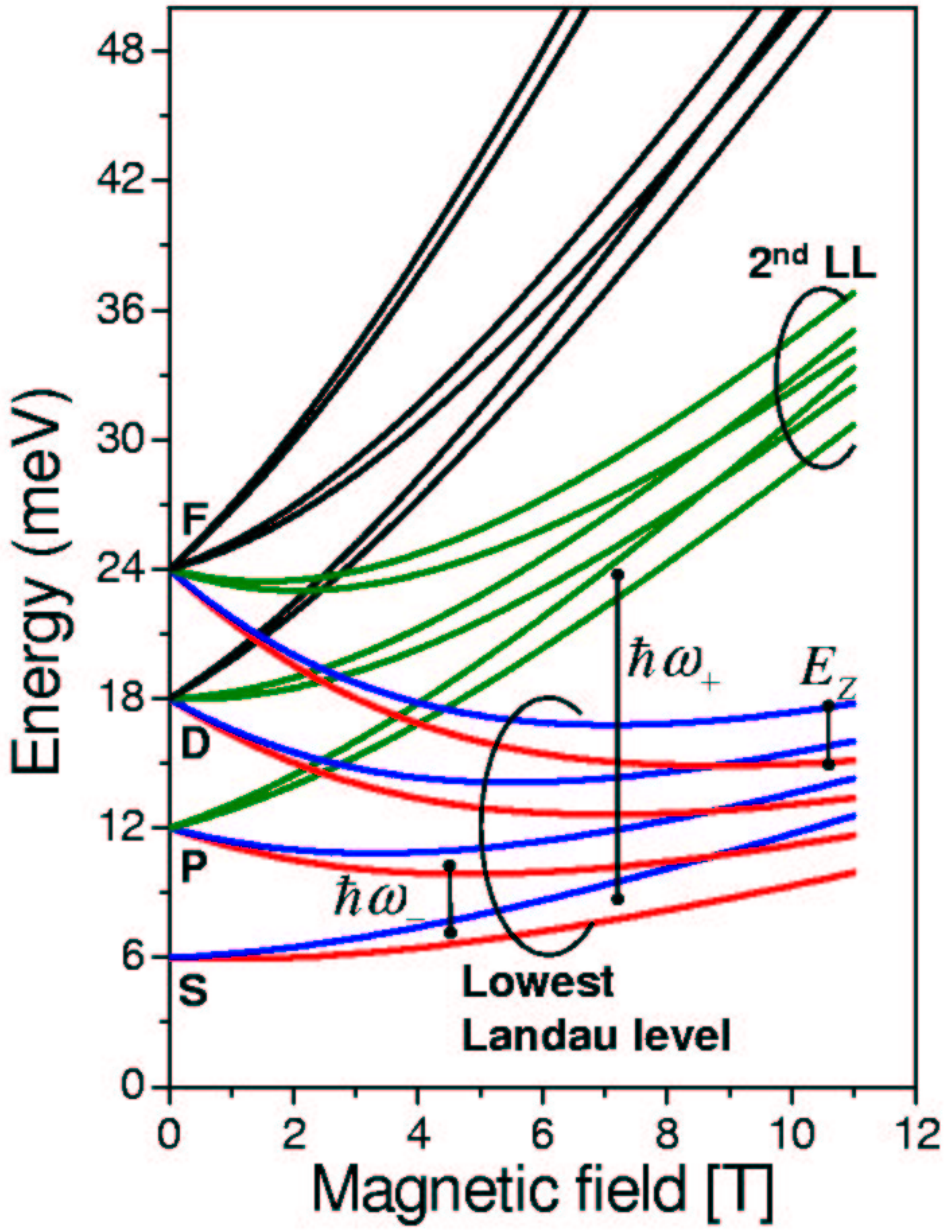

Figure 2.1: Energy spectrum of a single particle in a two-dimensional parabolic potential versus the magnetic field. I show the energies of twenty eigenstates which in the absence of the magnetic field form four lowest shells (see text for details). In this figure, the parabolic frequency $\hbar\omega_0 = 6$ meV, and the Landé factor $g = -4.4$.

states $(n, m) = (0, 1)$ and $(n, m) = (1, 0)$, both of them doubly degenerate with respect to spin. The third - d shell consists of states $(n, m) = (0, 2)$, $(1, 1)$, and $(2, 0)$, each of them spin-degenerate. Subsequent shells can be generated in analogous manner; the degeneracy of each next shell is greater by 2 than that of the previous shell (that includes the spin degeneracy). Moreover, the energy distance between consecutive shells is constant and equal to $\hbar\omega_0$.

As the magnetic field is increased, the frequency ω_+ increases, and the frequency ω_- decreases. Also, the Zeeman factor starts playing a role, causing the states with different spin orientations to differ in energies; this gap grows linearly with the magnetic field. Therefore, all degeneracies are removed, as seen in Fig. 2.1. In this Figure, in the lowest part of the spectrum I denote the spin-down states in red, and the spin-up states - in blue. This spin splitting occurs also for all higher states (accounted for in the graph, but not indicated with colours). Note that at certain values of the magnetic field (e.g., about 2 T and about 4 T) one sees crossings of levels belonging to different shells. In the absence of the Zeeman energy, this effect is observed whenever the ratio of frequencies $\omega_+/\omega_- = p/q$, where $p > q$ are nonzero integers.

For very large magnetic fields the frequency ω_- is very small (approaches zero), and the frequency ω_+ approaches the cyclotron frequency ω_c. At these fields the Landau level (LL) structure of the spectrum becomes particularly clear. The lowest Landau level (LLL) is composed of one pair of states from each shell (differing only by spin); these states are plotted in Fig. 2.1 in red and blue for spin down and up, respectively. A characteristic feature of all of these states is that all of them have the quantum number $n = 0$. The second LL (plotted in green) is composed again of one pair of states from each shell, but now with the exception of the s shell, whose states have already appeared in the LLL. All states here have the quantum number $n = 1$. In the Figure, one can also see a few lowest energies of states belonging to the third and fourth LLs, whose quantum numbers n are equal to 2 and 3, respectively. Each higher shell contributes to all LLs; I have presented

only four lowest shells for clarity. Since in the unmodified parabolic potential the number of shells is infinite, in reality each LL is composed of an infinite number of states. In this context let us note that the operators a, a^+ are associated with the frequency ω_+, and therefore they are respectively inter-Landau-level lowering and raising operators. The difference of energies of two corresponding states (i.e., with the same m and σ) belonging to two consecutive LLs is thus equal to $\hbar\omega_+$. Analogously, b, b^+ are associated with the frequency ω_-, and are respectively intra-Landau-level lowering and raising operators. The splitting between two consecutive levels in one LL, neglecting the Zeeman splitting, is equal to $\hbar\omega_-$.

Finally let us express the z component of the angular momentum operator in the language of the lowering and raising operators:

$$\hat{l}_z = -\frac{\hbar}{2}\left(z\partial_z - z^*\partial_z^*\right) = -\hbar(b^+b - a^+a). \tag{2.19}$$

The states $|nm\sigma\rangle$ are thus also eigenstates of the operator l_z with eigenvalues $\hbar l = \hbar(n-m)$. The z component of the angular momentum is thus a good quantum number (the corresponding operator $\hat{l}_z$ commutes with the Hamiltonian, and thus can be diagonalised together with it). In this context the degenerate structure of the p shell at zero magnetic field becomes more clear: the two doubly-spin-degenerate states have opposite angular momenta (1 and -1, respectively), and their degeneracy simply reflects the axial symmetry of the potential. In the d shell, however, there are *three* doubly-spin-degenerate levels. The degeneracy of two of them, with angular momenta 2 and -2, respectively, can be accounted for similarly to the states in the p shell. However, the third state, with angular momentum 0, does not fall into this category. Its degeneracy with the other two states in the d shell results from *dynamical* symmetries of the parabolic potential. These symmetries are similar to those in real atoms: atomic shells exhibit degeneracy which is higher than that due to the spherical symmetry of the system [35]. This is reflected in the fact that the energy of atomic levels depends only on one quantum number (the principal quantum number n).

The notion of angular momentum also allows for an interpretation of the raising and lowering operators: in acting on a state $|nm\rangle$ the operators a and a^+ respectively decrease and increase the angular momentum, thus they control the "counterclockwise" motion of an electron (to use a classical analogy). They also work against the magnetic field, which, in classical terms, accelerates the electron in the "clockwise" motion via the Lorenz force (this is because the magnetic field $\mathbf{B} = [0, 0, B]$ is parallel to the z axis and the electronic charge is negative). This is why Landau levels are composed of states with the same quantum number n: upon application of the operator a^+ the electron acquires one quantum of the "counterclockwise motion", which transfers it one LL up.

2.2 Confinement of the quantum disk

In this Section I shall find the single-particle energy spectrum of an electron confined in a potential of a quantum disk with infinite walls. Let us denote the disk thickness by W and the disk radius by R. The Hamiltonian of the system in an external magnetic field $\mathbf{B} = [0, 0, B]$ takes the form

$$\hat{H} = \frac{1}{2m^*}\left(\hat{\mathbf{p}} + \frac{e}{c}\hat{\mathbf{A}}\right)^2 + \tilde{V}(x, y, z) - g\mu_B B\sigma, \tag{2.20}$$

with all the symbols defined in Section 2.1. The potential $\tilde{V}(x, y, z)$ equals zero inside the disk, and infinity outside it. When expressed in cylindrical coordinates (ϱ, θ, z), this potential does not depend on the angle θ. Moreover, it can be separated into two parts:

$$\tilde{V}(\varrho, z) = \tilde{V}_R(\varrho) + \tilde{V}_Z(z), \tag{2.21}$$

each part dependent on one coordinate only. The potential $\tilde{V}_Z$ is that of a square quantum well with infinite walls, and the potential $\tilde{V}_R$ is that of a two-dimensional circular quantum well, also with infinite walls. Here I have assumed that the z axis coincides with the axis of rotational symmetry of the system.

At this point one can analytically obtain the energies and wave functions of an electron in the absence of the magnetic field, and this is what I shall do in the first part of this Section. The symmetry introduced by the magnetic field, however, turns out to be different than that of the disk potential, which makes it difficult to obtain an analytical solution in the presence of the magnetic field in a closed form. I shall therefore calculate the full single-particle energy spectrum as a function of the magnetic field using numerical methods. This procedure will be described in detail in the second part of this Section.

2.2.1 Quantum disk in the absence of the magnetic field

To simplify the notation, I will express all energies in units of the effective Rydberg, $\mathcal{R} = m^* e^4/2\varepsilon^2\hbar^2$, and all lengths in the units of the effective Bohr radius $a_B = \varepsilon\hbar^2/m^* e^2$ (ε is the dielectric constant of the QD material). For example, for GaAs $\varepsilon = 12.4$ and the effective mass of an electron $m^* = 0.067\, m_0$, which yields $1\,\mathcal{R} \approx 5.93$ meV and $1\,a_B \approx 97.9$ Å. In these units the Hamiltonian (2.20) with $B = 0$ and written in cylindrical coordinates attains the following form:

$$\hat{H} = \left[-\frac{1}{\varrho^2}\left(\varrho\frac{\partial}{\partial\varrho}\varrho\frac{\partial}{\partial\varrho} + \frac{\partial^2}{\partial\theta^2}\right) - \frac{\partial^2}{\partial z^2}\right] + V_R(\varrho) + V_Z(z) \tag{2.22}$$

(note that the coordinates ϱ and z are now dimensionless). The above Hamiltonian can be separated into two parts, one describing the motion in z direction, and one describing the radial and angular motion. To take advantage of this fact, I shall seek the full wave function in the form

$$\Psi(\varrho, \theta, z) = \Phi(\varrho, \theta)\xi(z),$$

i.e., as a product of the in-plane and the z-dependent parts. In this case the Schrödinger equation written with the Hamiltonian (2.22) splits into two equations:

$$\left[-\frac{1}{\varrho^2}\left(\varrho\frac{\partial}{\partial\varrho}\varrho\frac{\partial}{\partial\varrho} + \frac{\partial^2}{\partial\theta^2}\right)\right]\Phi(\varrho,\theta) + V_R(\varrho)\Phi(\varrho,\theta) = E_R\Phi(\varrho,\theta), \tag{2.23}$$

$$-\frac{\partial^2}{\partial z^2}\xi(z) + V_Z(z)\xi(Z) = E_Z\xi(z), \tag{2.24}$$

and the total energy $E = E_R + E_Z$.

Let us solve the equation (2.24) first. As I have already established, $V_Z(z)$ is the potential of a square quantum well with infinite walls. This problem is considered in many textbooks on quantum mechanics (see e.g. Ref [35]), and here I shall just write out its solution. For simplicity let us assume that the left wall of the well is positioned at $z = 0$, and the right wall - at $z = W$. In this case the normalised eigenstates of the equation (2.24) can be expressed by sines only (the wave functions do not contain cosine terms as they attain nonzero values at $z = 0$, i.e., at the edge of the well):

$$\xi_l(z) = \sqrt{\frac{2}{W}} \sin\left(\frac{l\pi}{W} z\right). \tag{2.25}$$

The corresponding eigenenergies are:

$$E_Z(l) = \frac{\pi^2}{W^2} l^2, \tag{2.26}$$

and the vertical quantum number $l = 1, 2, \ldots$.

Let us now move on to the equation (2.23). In this case one usually attempts to write the eigenfunction in the form

$$\Phi(\varrho, \theta) = R(\varrho) e^{im\theta}, \tag{2.27}$$

since the Hamiltonian of the planar motion contains elements of the z component of the angular momentum operator (m is the angular momentum quantum number). If one substitutes this wave function to Eq. (2.23), performs the differentiation and reduces the exponent on both sides, one obtains

$$\left[-\frac{1}{\varrho^2}\left(\varrho\frac{\partial}{\partial\varrho}\varrho\frac{\partial}{\partial\varrho} - m^2\right)\right] R(\varrho) + V_R(\varrho) R(\varrho) = E_R R(\varrho). \tag{2.28}$$

This equation becomes the Bessel equation if $V_R(\varrho) \equiv 0$. Let us assume so, and include the potential V_R later on. In this case the analytical solution of this equation is possible [1], and the resulting unnormalised wave functions attain the form

$$R_m(\varrho) = J_m(\sqrt{E_R}\varrho), \tag{2.29}$$

where J_m are the Bessel functions of order m, and m is the angular momentum quantum number.

Let us now include the potential $V_R(\varrho)$. This potential is equal to zero inside the disk (i.e., for $\varrho < R$, where R is the disk radius), and infinity on the outside (i.e., for $\varrho \geq R$). Therefore the acceptable wave functions must have a node at $\varrho = R$, i.e.,

$$R_m(\sqrt{E_R}R) = 0.$$

This gives the quantisation condition for energy, which is

$$E_R(n,m) = \left(\frac{\alpha_m^n}{R}\right)^2. \tag{2.30}$$

Here α_m^n denotes the n-th node of the Bessel function J of order m. In other words, one obtains an additional radial (or nodal) quantum number $n = 1, 2, 3, \ldots$, which, together with the angular momentum quantum number m, defines modes of the planar motion. The nodes α_m^n are obtained numerically.

The eigenenergies and normalised eigenfunctions of the total Hamiltonian (2.22) can now be written as:

$$E(n,m,l) = \left(\frac{\alpha_m^n}{R}\right)^2 + \frac{\pi^2}{W^2}l^2, \tag{2.31}$$

$$\langle\vec{r}|nml\rangle = \frac{\sqrt{2}}{R}\frac{1}{|J_{m+1}(\alpha_m^n)|}J_m\left(\frac{\alpha_m^n}{R}\varrho\right)\cdot\frac{1}{\sqrt{2\pi}}e^{im\theta}\cdot\sqrt{\frac{2}{W}}\sin\left(\frac{l\pi}{W}z\right). \tag{2.32}$$

Note that the quantum numbers n, m defining the eigenenergies and eigenvectors of the disk potential, although named with the same letters, have a *different* interpretation than the numbers n, m used in the case of parabolic confinements. Here, n_{disk} can be considered as the number of nodes in the radial direction, and $\hbar m_{disk}$ is the angular momentum of a given single particle state. In the parabolic case, n and m denoted the number of quanta of the "counterclockwise" and "clockwise" motion, respectively, and the angular momentum of a given state had to be calculated as $\hbar l = \hbar(n-m)$.

To complete the description of the case of zero magnetic field, let us briefly discuss the obtained energy spectrum. The formula (2.31) consists of two parts: first, corresponding

to the radial confinement, and second, corresponding to the vertical confinement. The first part scales as R^{-2}, and the second part as W^{-2}. Since the disk height W is usually much smaller than the disk radius R (for typical disk-shaped InAs/GaAs QDs, $R \approx 80$ Å and $W \approx 20$ Å), the energy gaps between states with different numbers l, but the same n, m are much larger than the gaps between states with different numbers n, m, but the same l. Thus the spectrum consists of widely-spaced *subbands*, corresponding to different values of l, on top of which there are different modes of lateral motion, spaced much more closely. These modes are also organised in degenerate shells, and to demonstrate this let us write out values of $E_R(n,m)$ for several sets of quantum numbers (n,m). Assuming that the disk radius $R = 1\ a_B$, and using the values of Bessel zeros available in literature [1], one obtains: $E_R(0,0) = 5.783\ \mathcal{R}$ (s shell); $E_R(0,1) = E_R(0,-1) = 14.682\ \mathcal{R}$ (p shell); $E_R(0,2) = E_R(0,-2) = 26.375\ \mathcal{R}$ and $E_R(1,0) = 30.471\ \mathcal{R}$ (d shell). All these states are doubly degenerate with respect to spin. Note that here the p shell is also orbitally degenerate, as is the case with the parabolic potential. The d shell, on the other hand, is only partially orbitally degenerate. I shall discuss this and other properties of this spectrum at the end of this Section, together with effects introduced by the magnetic field.

2.2.2 Quantum disk in finite magnetic fields

Let us now consider the Hamiltonian (2.20) in nonzero magnetic field, but for now omitting the Zeeman term. If the vector potential $\mathbf{A}$ is chosen in the symmetric gauge: $\mathbf{A} = [-By/2, Bx/2, 0]$, this Hamiltonian can be written as a sum

$$\hat{H}(B) = \hat{H}(0) + \frac{1}{8}m^*\omega_c^2 r^2 + \frac{1}{2}\omega_c \hat{l}_z, \tag{2.33}$$

where $\hat{H}(0)$ denotes the Hamiltonian (2.22) in the absence of the magnetic field, and the meaning of all other symbols is identical to that introduced in the case of the parabolic potential in Section 2.1. Thus, there are two terms dependent upon the magnetic field:

the first one depends on B quadratically, and the second one - linearly. To proceed further, let us write the above Hamiltonian in dimensionless units:

$$\hat{H}(B) = \hat{H}(0) + \frac{1}{16}\Omega_c^2\varrho^2 - \frac{i}{2}\Omega_c\frac{\partial}{\partial\theta}, \tag{2.34}$$

where $\Omega_c = \hbar\omega_c/\mathcal{R}$ is the dimensionless cyclotron energy. Note that the terms dependent upon the magnetic field directed along the z axis do not depend on the z coordinate, but affect only the planar motion of the particle.

To find eigenenergies and eigenstates of the Hamiltonian (2.34), I shall use the exact diagonalisation procedure. This procedure involves: (i) choosing a basis of single-particle states, (ii) writing the Hamiltonian in matrix form in this basis, and (iii) diagonalising this Hamiltonian matrix numerically.

As for the choice of basis, the eigenstates $|nml\rangle$ (Eq. (2.32)) of the zero-field Hamiltonian $\hat{H}(0)$ seem to be natural candidates. But I do not have to build my basis out of states with all possible values of n, m and l; I can divide my basis into subsets, containing functions with defined m and l, but with various n. To see why I can do that, let us check how the Hamiltonian (2.34) acts on a function $|nml\rangle$. I have $\hat{H}(0)|nml\rangle = E(n,m,l)|nml\rangle$, with $E(n,m,l)$ defined by Eq. (2.31), because these states are eigenstates of the zero-field Hamiltonian. Further, for the last term of the Hamiltonian (2.34) I get

$$-\frac{i}{2}\Omega_c\frac{\partial}{\partial\theta}|nml\rangle = \frac{m}{2}\Omega_c|nml\rangle,$$

which is readily seen from the form of the function $|nml\rangle$ (Eq. (2.32)). Finally, the action of the second term of $\hat{H}(B)$ on $|nml\rangle$ can be written in the operator form,

$$\frac{1}{16}\Omega_c^2\varrho^2|nml\rangle.$$

Let us now analyse the three expressions. In all three cases the part of the function describing the motion in z direction is left unchanged - in other words, the Hamiltonian $\hat{H}(B)$ does not couple states with different quantum numbers l. The angular part of the wave function is not affected either - $\hat{H}(B)$ does not couple states with different quantum

numbers m (in other words, the magnetic field directed along the z axis conserves the z component of the angular momentum of the particle). The only part of $|nml\rangle$ not conserved by $\hat{H}(B)$ is the radial part, and this is due only to the second term (the one containing ϱ^2). Therefore in choosing my basis I can preset the desired angular momentum m and the quantum number l, and take states with all possible radial quantum numbers n. Thus, my basis consists of states $\{|1ml\rangle, |2ml\rangle, |3ml\rangle, \ldots\}$.

In the second step of the procedure, I write the Hamiltonian $\hat{H}(B)$ in matrix form in the chosen basis. The matrix elements of this Hamiltonian are

$$\langle lmn_1|\hat{H}(B)|n_2ml\rangle = E(n,m,l)\delta_{n_1,n_2} + \frac{1}{16}\Omega_c^2\langle lmn_1|\varrho^2|n_2ml\rangle + \frac{m}{2}\Omega_c\delta_{n_1,n_2}, \qquad (2.35)$$

where δ_{n_1,n_2} is the Kronecker delta ($\delta_{n_1,n_2} = 1$ if $n_1 = n_2$, and zero otherwise). This expression is obtained by collecting all the terms considered earlier, when I analysed how $\hat{H}(B)$ acts on $|nml\rangle$, and taking into account the fact that the functions $|nml\rangle$ form an orthonormal set.

Note that the first and the third term appears only on the diagonal of the Hamiltonian matrix, while the second term introduces both diagonal and off-diagonal matrix elements. This term, written explicitely, has the form

$$\langle lmn_1|\varrho^2|n_2ml\rangle = \frac{2}{R^2}\frac{1}{|J_{m+1}(\alpha_m^{n_1})J_{m+1}(\alpha_m^{n_2})|}\int_0^R d\varrho\varrho^3 J_m\left(\frac{\alpha_m^{n_1}}{R}\varrho\right)J_m\left(\frac{\alpha_m^{n_2}}{R}\varrho\right).$$

This integration has to be carried out numerically.

Thus, I have defined my basis and I have calculated the Hamiltonian matrix elements in this basis. Before I can proceed to the proper diagonalisation, note that my basis is infinite, and therefore my Hamiltonian is also a matrix of infinite dimension. Thus, to be able to carry out calculations I need to restrict my basis to a finite set, or, in other words, limit the region of radial quantum numbers n. To decide how to do it, I invoke the rules of perturbation analysis [35] defining the subsequent corrections to the energy coming from mixing between basis states. These corrections are always in the form of a ratio, whose numerator contains the matrix elements of the perturbed Hamiltonian, and the denomina-

tor - respective differences of eigenenergies of the unperturbed Hamiltonian. This means in practice that in calculating the ground state energy of the Hamiltonian $\hat{H}(B)$ it is appropriate to choose a basis consisting of several low-lying levels $|nml\rangle$ of $\hat{H}(0)$; corrections from higher energies should give small contribution to the energy. Therefore, I choose the maximal quantum number n_{max}, which will be my cutoff, and the basis $\{|nml\rangle\}$ will now be finite and will contain only states with $1 \leq n \leq n_{max}$. There still remains a question of how much should n_{max} be to guarantee a well-converged result. The most straightforward method of establishing the cutoff value involves diagonalising the Hamiltonian in several bases (with different values of n_{max}) and performing the convergence study. This method will be used in my case.

I am now ready for the third step of the procedure - the diagonalisation of the Hamiltonian matrix. This is a standard operation of linear algebra, and many software packages capable of performing it are available. Calculations presented here are done using the Linear Algebra Package (LAPACK) [71] prepared as a FORTRAN software library.

For my model calculations I use a disk potential with thickness $W = 20$ Å and radius $R = 200$ Å. Note that the radius is taken to be more than two times larger than typical radii of indium-flushed InAs QDs on GaAs substrate (for these structures typically $R \approx 80$ Å), but comparable to the radii of InAs QDs grown on InP substrate. I took such a large radius of the structure to make the magnetic-field-induced effects more visible, since for small disks the field-dependent corrections in $\hat{H}(B)$ are small compared to the energy quantisation introduced by $\hat{H}(0)$.

First let us examine the convergence of the ground state energy in the channel $m = 0$, $l = 1$ (i.e., zero angular momentum, lowest subband of the vertical motion) as a function of the basis size. Since the magnetic terms in $\hat{H}(B)$ increase with increasing magnetic field, I perform my control calculations for a large field, e.g., for $B = 10$ T; if the result has converged for this field, it will also be well-converged for smaller fields. For my model structure at $B = 10$ T, I have performed calculations with n_{max} ranging from 1 to 20.

n_{max}	$E_{GS}(m=0, l=1, B=10\,\mathrm{T})$ (eV)
1	1.41420722313
2	1.41406380561
3	1.41406291665
4	1.41406283691
5	1.41406282464
6	1.41406282195
7	1.41406282120
8	1.41406282095
9	1.41406282085
10	1.41406282081
15	1.41406282078
20	1.41406282077

Table 2.1: Convergence of the ground-state energy for angular momentum $m = 0$ and the vertical quantum number $l = 1$ of a quantum disk with $W = 20$ Åand $R = 200$ Å

The ground-state energies with $m = 0$ and $l = 1$ obtained in each case are shown in Table 2.1. As can be seen, the convergence is achieved very rapidly, so that the result is fully converged already for $n_{max} = 20$. I choose this cutoff of the basis in my further calculations. Note that for a disk with $W = 20$ Å and $R = 80$ Å the convergence is expected to occur for even smaller n_{max}, since the quantisation introduced by the zero-field Hamiltonian $\hat{H}(0)$ is more than four times stronger than that with $R = 200$ Å(indeed, the result is already fully converged for $n_{max} = 5$).

Using the exact diagonalisation procedure I have calculated several low-lying energy levels for my disk structure as a function of the magnetic field for $l = 1$ and in angular

momentum channels $m = 0, \pm 1, \pm 2, \pm 3$. Results of my calculations are shown in Fig. 2.2. I shall discuss the fundamental features seen in this graph by comparing it to Fig. 2.1, where I presented the spectrum corresponding to the parabolic potential.

Let us first focus on the case of zero magnetic field. As I already mentioned, the energy levels of the disk are organised in shells. The lowest shell - the s shell - is doubly degenerate with respect to spin, and the next shell - p - consists of four states, degenerate both orbitally and with respect to spin. These two shells behave identically as in the parabolic case, and the degeneracy of the p shell can be traced to the axial symmetry of the system. However, the d shell is only partially degenerate: the states with $m = \pm 2$ form a quadruplet, with both orbital and spin degeneracy present, but the doubly-spin-degenerate state with $m = 0$ lies at a slightly higher energy. Therefore, the disk potential does not exhibit the dynamical symmetries apparent in the parabolic confinement. The f shell is also split into two quadruplets: one with $m = \pm 3$ and one with $m = \pm 1$, all spin-degenerate. As can be seen, at zero magnetic field states with opposite angular momenta have the same energy, but there is *no* degeneracy of states with different angular momenta. Note also that the energy distance between consecutive shells in the case of my disk is larger than it is in the case of the parabolic system considered in Section 2.1. This is due to the fact that in the case of the disk the radial quantisation is stronger than that of the larger parabolic confinement. In fact, as I already mentioned, in more realistic approximations of indium-flushed quantum disks the radii are usually taken to be a factor of 2 smaller than the one I took. This makes the intershell gaps more than four times larger than those seen in Fig. 2.2. Also, all the energy levels on this graph correspond to states with the vertical quantum number $l = 1$. The states from the second subband are ignored, as their energies are much higher: due to the small disk width W one expects the second subband (containing states with $l = 2$) to start at energies of order of 5.6 eV.

Let us now move on to finite magnetic fields. Here I shall explicitely include the Zeeman term in the Hamiltonian, neglected up to now. Thus, I explicitely account for

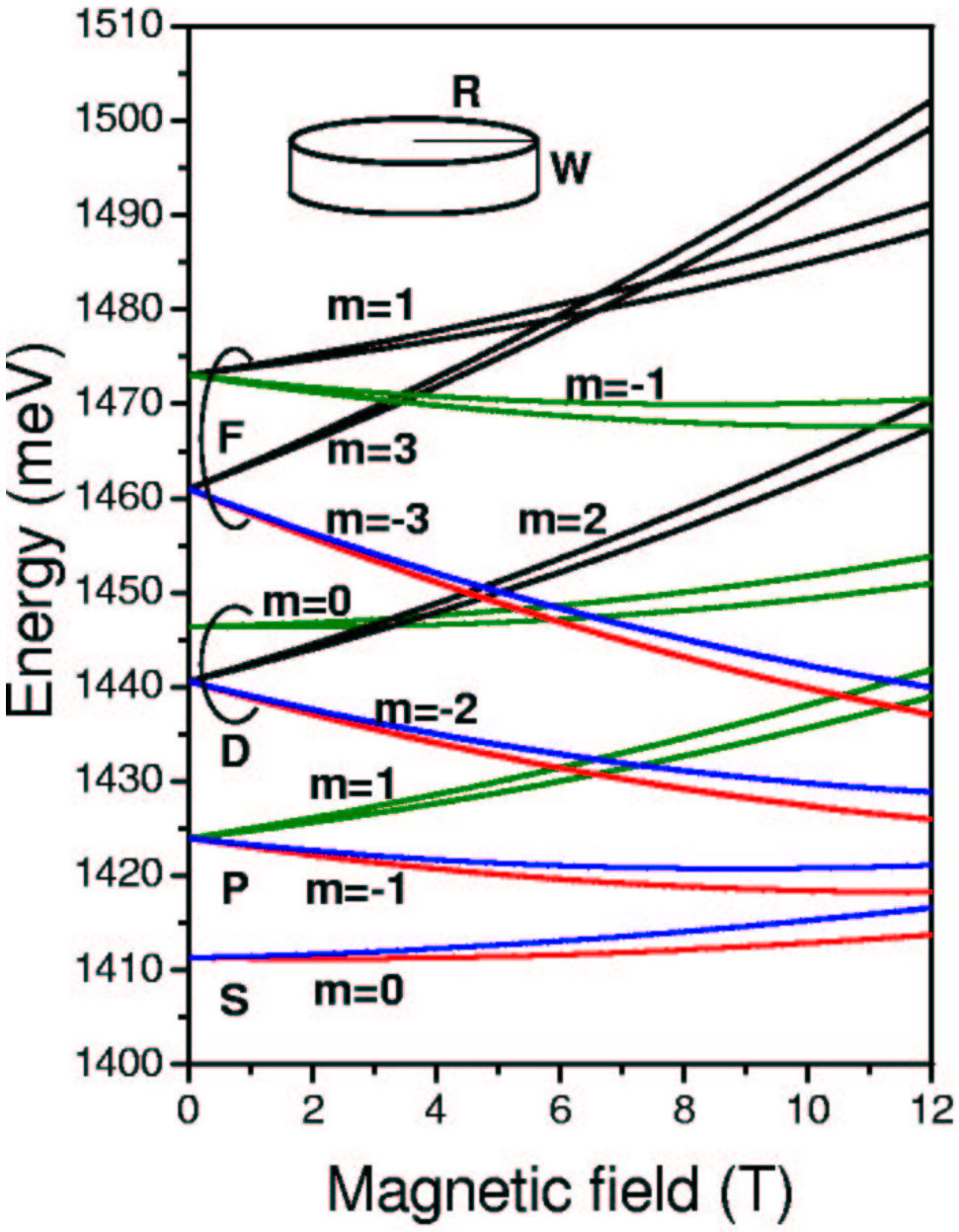

Figure 2.2: Energy spectrum of a single particle in a rigid-wall quantum disk potential versus the magnetic field. The width of the disk is $W = 20$ Å, and its radius is $R = 200$ Å. I show the energies of twenty eigenstates which in the absence of the magnetic field form four lowest shells (see text for details). In this figure the Landé factor $g = -4.4$. Inset shows the geometry of the disk confinement

the different possible values of electronic spin s_z; the spin quantum number σ becomes an additional good quantum number. The qualitative behaviour of the levels in Fig. 2.2 is similar to that in the parabolic confinement: the shell degeneracy - both orbital and spin - is removed. As I did in Section 2.1, here also I artificially enhanced the Zeeman energy to make it visible on this energy scale. Compared to the parabolic confinement, in the case of quantum disk the magnetic field has a smaller effect: in Fig. 2.1, at $B = 11$ T the structure of Landau levels was already well established, while here the states belonging to different Landau levels are still interspersed. In Fig. 2.2, the states forming the lowest LL are drawn with red and blue lines (to denote the spin down and up, respectively), and the states belonging to the second LL - with green lines. The weaker effect of the magnetic field is due to the stronger zero-field quantisation of the disk confinement: the magnetic corrections in the softer parabolic potential of large gated QDs contribute more strongly to the energy spectrum. Calculations made for the more realistic disk potential (with $R = 80$ Å, not shown here) show that there the magnetic field has even less effect: even at fields as large as 12 T the structure of the spectrum resembles more the split zero-field shells than Landau levels.

2.3 Confinement of the quantum ring

I shall now move on to discussing the last "ideal" single-particle potential - a quantum ring. Let us write the Hamiltonian for this system in a general form:

$$\hat{H} = \frac{1}{2m^*}\left(\hat{\mathbf{p}} + \frac{e}{c}\mathbf{A}\right)^2 + V_R(x, y, z). \tag{2.36}$$

Henceforth I shall omit the Zeeman term, since, as I have already demonstrated, it changes the single-particle spectra only in a minor way. As for the quantum-ring potential $V_R(x, y, z)$, for simplicity I shall take it to be the ring-shaped quantum well with infinitesimal thickness and width, and infinite walls. In other words, $V_R(x, y, z) \equiv V_R(\varrho, \theta, z)$ restricts the motion of the electron only to the region defined by $\varrho = R$ and $z = 0$ (the

circumference of a circle, where R is its radius). Moreover, as usual, I take the magnetic field $\mathbf{B}$ to be directed along the z axis, and the corresponding vector potential $\mathbf{A}$ in the symmetric gauge. In this situation it is natural to work in polar coordinates, in which the electronic motion is described by only one independent coordinate - the angle θ.

If one expresses the Hamiltonian (2.36) in these coordinates, one obtains:

$$\hat{H} = -\frac{\hbar^2}{2m^* R^2}\frac{\partial^2}{\partial\theta^2} + \frac{1}{8}m^*\omega_c^2 R^2 - \frac{i}{2}\hbar\omega_c\frac{\partial}{\partial\theta}. \tag{2.37}$$

I now define the magnetic length as $\ell = \sqrt{\hbar/m^*\omega_c}$. This allows me to write the Hamiltonian in the form

$$\hat{H} = \frac{\hbar^2}{2m^* R^2}\left(-i\frac{\partial}{\partial\theta} + N_\phi\right)^2, \tag{2.38}$$

where N_ϕ is the number of magnetic flux quanta threading the ring. This quantity is defined as $N_\phi = \pi R^2/2\pi\ell^2$ and is the ratio of the area of the ring to the area defined by the magnetic length. Since the magnetic length $\ell \sim B^{-1/2}$, the number of flux quanta increases linearly with the magnetic field.

The eigenstates of the Hamiltonian (2.38) are

$$\Psi_m(\theta) = \frac{1}{\sqrt{2\pi R}}e^{im\theta}, \tag{2.39}$$

where the angular momentum quantum number $m = 0, \pm1, \pm2, \ldots$. The corresponding eigenenergies are then $E(m) = \frac{\hbar^2}{2m^* R^2}(m + N_\phi)^2$, or in the effective Rydberg units, $E(m) = \frac{1}{R^2}(m + N_\phi)^2$ (now the ring radius R is expressed in the effective Bohr radii a_B). As can be seen from these formulae, the energy of a state with given angular momentum m depends quadratically on the magnetic field. This is seen in Fig. 2.3, where I show the quantity $E_m R^2$ as a function of the number of flux quanta N_ϕ for several angular momenta m. The colour lines show energies of states with definite angular momenta m (the values of m for each curve are given by the number on the graph). I deal thus with a series of parabolas, with minima at integer values of the number of flux quanta N_ϕ. These parabolas cross at half-integer values of N_ϕ. Therefore the single-electron ground-state energy, denoted in the graph by the black line, exhibits oscillations as a function of the

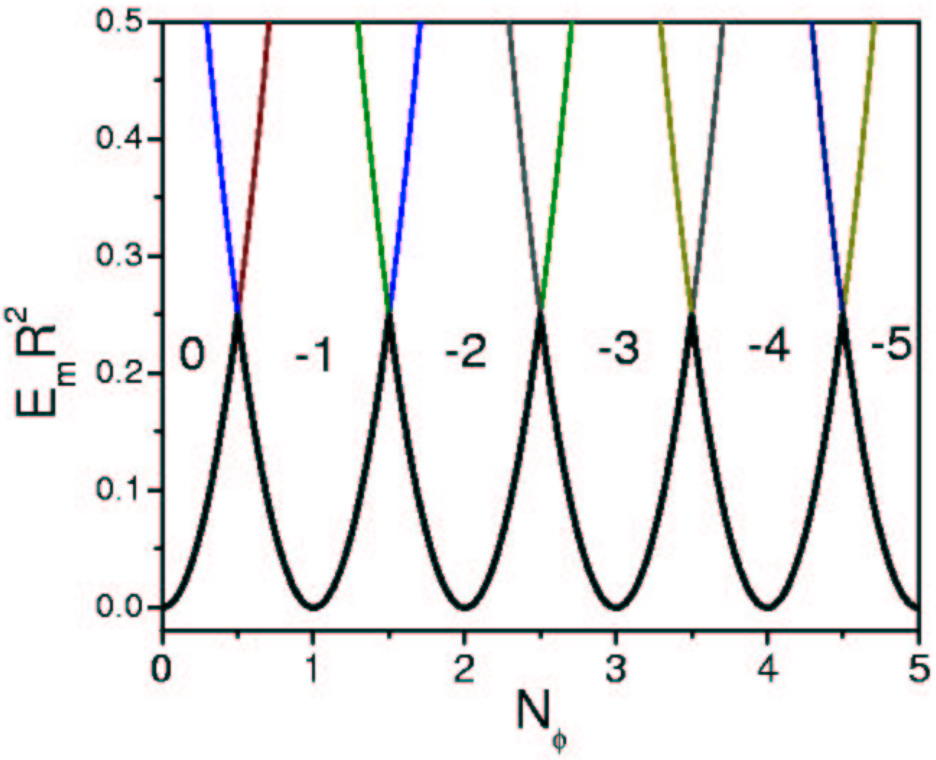

Figure 2.3: Energy of a single electron confined in a quantum-ring potential as a function of the number of flux quanta. The colour lines show energies of states with definite angular momenta m (given by numbers on the graph); the black line shows the ground-state energy

magnetic field. This is the Aharonov-Bohm effect. Note that at each maximum of the energy there is a transition in the ground state. At these points the angular momentum of the ground state changes by one unit (in the case of electrons it becomes more negative). This behaviour is fundamentally different from that observed in the energy spectra of the parabolic and the disk confinements. There the ground state was always the same (it was the state belonging to the s shell), and its energy depended monotonically on the magnetic field (see Figs. 2.1 and 2.2).